J. Synchrotron Rad. (1995). **2**, 99–105

Surface-Sensitive XAFS in the Hard X-ray Region with Sub-Monolayer Sensitivity

Hiroyuki Oyanagi,[a] Ryu Shioda,[a] Yuji Kuwahara[b] and Koukichi Haga[c]

[a]Electrotechnical Laboratory, Umezono, Tsukuba-shi, Ibaraki 305, Japan, [b]The Institute of Physical and Chemical Research, Wako-shi, Saitama 351-01, Japan, and [c]Sumitomo Electric Industries Ltd, 1 Taya-cho, Sakae-ku, Yokohama 244, Japan

(*Received 15 August 1994; accepted 23 January 1995*)

Surface-sensitive X-ray absorption fine structure (XAFS) with sub-monolayer sensitivity based on grazing-incidence fluorescence detection is reported. The efficiency of fluorescence detection increased by more than two orders of magnitude by combining a multipole wiggler with a multi-element Si(Li) solid-state detector. The capability of the present technique for structural studies of surfaces and buried interfaces in the hard X-ray region was demonstrated by As *K*-edge XAFS studies of the InP(001) surface exposed to AsH_3 flow. The results indicated that ~0.1 monolayer As atoms are incorporated into the surface replacing the P atoms.

Keywords: surface-sensitive XAFS; EXAFS; multipole wiggler; sub-monolayer sensitivity.

1. Introduction

For structural studies of surfaces and interfaces for multi-component systems, the information on the local structure around a particular species of atom is essential. X-ray absorption fine structure (XAFS) is a powerful technique for local structure determination. In the hard X-ray region (>4 keV), however, because of a large penetration depth, conventional XAFS experiments in transmission mode are far from surface sensitive. In order to apply XAFS to surfaces and buried interfaces, a surface-sensitive alternative measurement technique is required. Fluorescence detection is a highly sensitive monitoring technique of XAFS (Jaklevic *et al.*, 1977). A surface-selective fluorescence excitation has been achieved using grazing-incidence geometry (Becker, Golovchenko & Patel, 1983). Although the capability of surface-sensitive XAFS based on grazing-incidence fluorescence detection has been demonstrated (Heald, Keller & Stern, 1984), the application was limited to either non-crystalline or polycrystalline specimens because a conventional detector cannot eliminate substrate effects.

A surface-sensitive XAFS measurement has been established by energy discrimination of the fluorescence signal. It has been shown that epitaxial layers on single-crystal substrates can be studied with monolayer sensitivity (Oyanagi *et al.*, 1988). However, experiments using a single-element solid-state detector and bending-magnet radiation were not practical since a typical extended X-ray absorption fine structure (EXAFS) scan for a sample with 1 monolayer (ML) coverage took several hours (Oyanagi *et al.*, 1988). To make sub-monolayer experiments feasible, the total fluorescence yield should be increased by several orders of magnitude. A high-brilliance X-ray beam from a multipole wiggler and a multi-element solid-state detector can increase the total fluorescence yield. In this paper, we report surface-sensitive XAFS using a 27-pole wiggler and a 7-element solid-state detector applied to the incorporation process of group V atoms.

Recently, adsorption and desorption processes of group V elements have attracted much attention for understanding the incorporation problem during the fabrication of III–V semiconductor heterointerfaces using a low-pressure gas decomposition growth technique such as metal–organic vapor-phase epitaxy. Using grazing-incidence fluorescence XAFS, we have studied InP(001) surfaces after exposure to AsH_3 flow. The local structure of a trace amount (~0.1 ML) of As atoms incorporated in InP was successfully analyzed. The As *K*-EXAFS results show that the local distortion around the incorporated As atoms consists essentially of isotropic displacements of the nearest-neighbor In atoms along the [111] direction. The results will be discussed in relation to the As impurities in InP and the strained InAs monolayer on InP(001).

2. Experimental

2.1. *Surface-sensitive XAFS*

Fig. 1 shows a schematic representation of surface-sensitive XAFS where θ is the angle of incidence and δ_c is the critical angle for total reflection. It is well known that the interferences among the outgoing photoelectron waves (1), singly scattered waves (1–2) and doubly scattered waves with the shortest path length (1–2–1) give rise to EXAFS oscillations. Fluorescence detection is widely used as a means to record the modulation of the absorption coefficient for a dilute system or a thin film (Jaklevic *et al.*, 1977). However, this technique is not surface sensitive in the hard X-ray region since the penetration depth of

the incident beam and the escape depth of the emitted fluorescence are much greater than the layer thickness of interest. Below the critical angle for total reflection ($\theta < \delta_c$), X-rays are totally refracted as they cross the interface between the two media reducing the extinction length by several orders of magnitude. Using grazing-incidence geometry and energy discrimination of the fluorescence spectra, surface sensitivity can be dramatically improved.

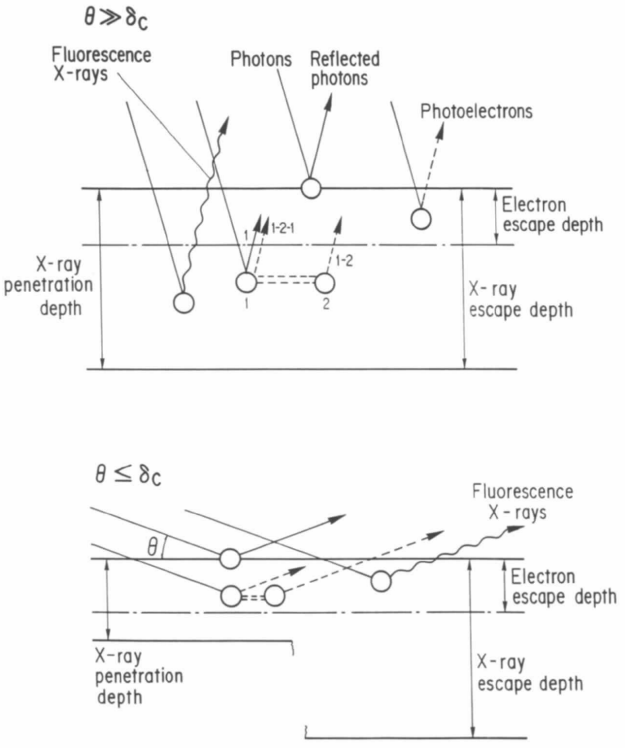

Figure 1
Schematic representations of normal (top) and surface-selective (bottom) fluorescence excitation. Grazing-incidence geometry can reduce the probing depth by several orders of magnitude, achieving a surface-selective excitation.

In Fig. 2, the experimental set-up for surface-sensitive XAFS with grazing-incidence fluorescence detection is schematically illustrated. The white X-ray beam from a multipole wiggler is monochromated by a fixed-exit double-crystal monochromator which horizontally focuses the output beam by sagittal bending of the second crystal. For vertical focusing and the rejection of higher harmonics, a bent Pt-coated fused-quartz mirror is used behind the monochromator. The reflectivity of semiconductor single crystals sharply varies around δ_c. A typical critical angle in the hard X-ray region is several milliradians. For example, δ_c for silicon at 12.3 keV is ~3.5 mrad. In order to control the angle of incidence θ around δ_c, a high-precision goniometer was used with a minimum step of 6.3 μrad. Both fluorescence X-ray and the reflected beam intensity were monitored to determine a proper θ value. The vertical divergence of the incident beam is limited by the slits (~50 μm) placed in front of the beam monitor and only a central region of a specimen (10 × 15 mm) was irradiated. For the polarization-dependent measurement, a sample is flipped by 90° around the axis of the incident beam. Vertical and horizontal sample orientations provide information on the radial distributions around an excited atom parallel and perpendicular to the surface normal, respectively. Fluorescence lines due to the substrate, such as In $L\alpha$, were absorbed by aluminium foils inserted between the detector and the sample. The discriminator levels of the detector electronics were chosen so that only the As $K\alpha$ line was counted as a function of photon energy.

2.2. *Multipole wiggler*

Experiments were performed at beamline BL13 of the Photon Factory. A 27-pole wiggler magnet (Sasaki, Yamamoto, Shioya & Kitamura, 1989) inserted in a straight

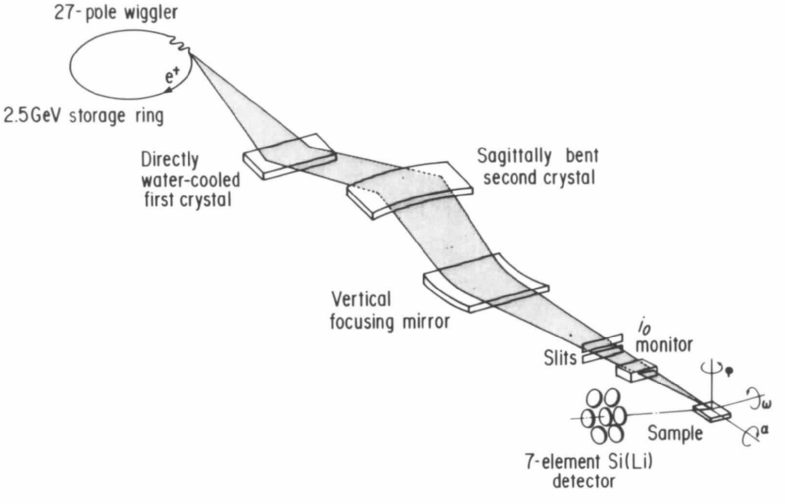

Figure 2
Arrangement for surface-sensitive XAFS experiments in grazing-incidence fluorescence detection. A sample is flipped by 90° for polarization dependence to analyze anisotropic structure.

section of the 2.5 GeV storage ring was used as a light source. The total calculated power of the multipole wiggler is 5.44 kW with the maximum magnetic field B_0 = 1.5 T. Fig. 3 shows that the calculated brilliance of the multipole wiggler is greater than that of a bending magnet roughly by an order of magnitude extending over a wide energy range (4–30 keV) where the K- and L-absorption edges for atoms with $Z > 20$ are distributed. The high heat load of the multipole wiggler, however, causes a serious problem which degrades the throughput and angular divergence of the monochromated X-ray beam (Oversluizen *et al.*, 1989). White X-rays pass through the water-cooled graphite absorbers (130 μm × 5) and the Be windows (200 μm × 2), absorbing 30–50% of the heat load which impinges on the first crystal. A directly water-cooled Si(111) crystal was used (Oversluizen *et al.*, 1989). The horizontal acceptance of the X-ray optics (~4 mrad) is sagittally focused to a 4 mm (H) × 1 mm (V) spot at a point ~36 m away from the source point (3:1 focusing). For the As K-EXAFS measurements for AsH_3-exposed InP, the unfocused beam was used.

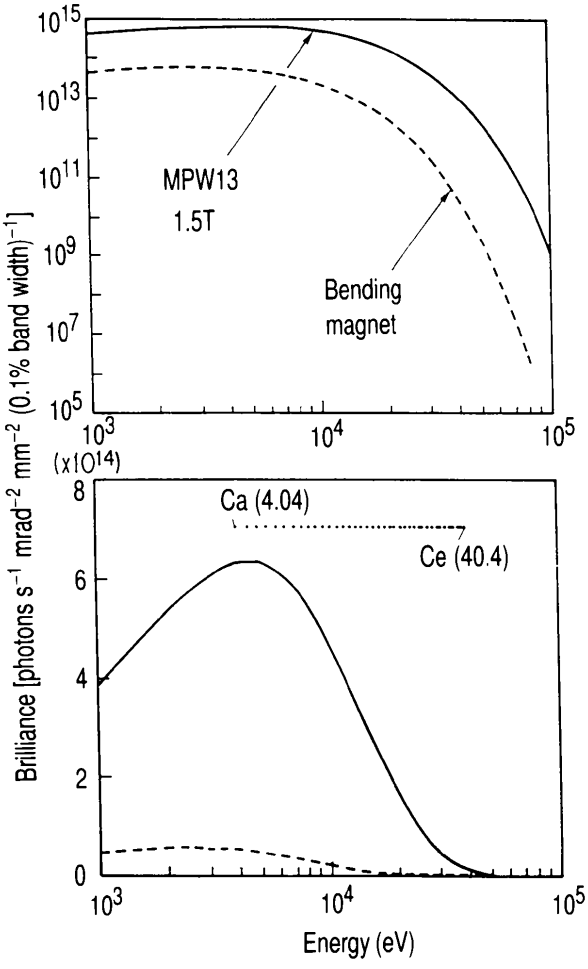

Figure 3
Calculated brilliance of a 27-pole wiggler magnet in comparison with that of a bending magnet on a logarithmic scale (above) and on a linear scale (bottom). The positions of the absorption edges for elements with $Z > 20$ are indicated.

2.3. *Sample preparation*

The incorporation process of As atoms into InP was studied by As K-EXAFS for the InP(001) surface exposed to AsH_3 flow. Source materials for the normal metal–organic vapor-phase-epitaxy growth of InAsP layers were trimethylindium, AsH_3 and PH_3 (Kamei & Hayashi, 1991). As a buffer layer, a 1000 Å thick InP layer was grown prior to exposure to AsH_3. The InP(100) substrates were exposed to the AsH_3 flow at 893 K for a short period (0.5 s) whilst maintaining the PH_3 flow. The flow rates for AsH_3 and PH_3 were 2 and 20 standard cm^3, respectively. A 20 Å thick InP cap layer was grown on top to protect the surface from degradation after the exposure to AsH_3 and during the cooling process. The As coverage (~0.1 ML) was estimated from both the intensity of the As $K\alpha$ fluorescence line and chemical analysis using inductively coupled plasma mass spectroscopy (ICPMS).

3. Results

The cooling efficiency of a grooved silicon crystal was improved by replacing a conventional semicircular cooling channel (Oversluizen *et al.*, 1989) with a flat one (Oyanagi, 1992). Details of the directly cooled crystal will appear elsewhere (Oyanagi, Kuwahara, Yamaguchi & Shioda, 1995). Using the optimized first crystal, the energy resolution $\Delta E/E \simeq 2 \times 10^{-4}$ was obtained for $B_0 < 1.25$ T. This energy resolution was sufficient for practical XAFS experiments. For higher magnetic fields, the full width at half maximum of the rocking curve still increased.

The fluorescence spectrum for the InP(001) surface after exposure to AsH_3 flow measured using grazing-incidence geometry is shown in Fig. 4. On decreasing the incidence angle θ, the intensity of the elastic peak drops and the signal-to-background ratio sharply increases for $\theta < \delta_c$. However, the elastically scattered incident beam still dominates the spectrum. The As $K\alpha$ fluorescence line corresponding to ~0.1 ML is observed as a weak peak on the lower-energy side. It should be noted that the present signal-to-background ratio (~0.25) would be improved by a factor of five if a Ge X-ray filter is used. The As K-fluorescence yield spectrum normalized by the incident beam intensity measured by an ionization chamber is shown in Fig. 5. A typical count rate per channel for 0.1 ML As is approximately 10^3 counts s^{-1} above the absorption edge. The spectrum shown in Fig. 5 was obtained by averaging six scans of 7-channel data integrated for 10 s. The total 7 × 10^4 counts were integrated for each data point.

In Fig. 6, the normalized As K-EXAFS oscillations are shown for 0.1 ML As/InP together with the data for As impurities in InP, referred to As:InP (Oyanagi *et al.*, 1988) and InAs powder measured in a transmission mode as a function of photoelectron wavenumber k. The careful analysis of EXAFS spectra for InAs powder measured in fluorescence and transmission modes confirmed that the data taken by these two modes can be quantitatively compared. Efforts

were made to estimate the proper background function due to atomic absorption. A well known Victoreen formula was normalized to the magnitude of the absorption edge. The backscattering amplitude $|f_i(\pi, k)|$ for In has a large value in the low-k region and a minimum at $k = \sim 7$ Å^{-1}, in sharp contrast with As atoms for which $|f_i(\pi, k)|$ has a maximum at $k = 6$–7 Å^{-1} and extends to $k > 15$ Å^{-1}. The k-dependence of EXAFS oscillations for 0.1 ML As/InP is quite similar to those for As:InP both in phase and amplitude. For As:InP, As impurities substitute anion (P) atom sites of a zincblende structure. It is concluded that the As atoms in 0.1 ML As/InP are tetrahedrally coordinated, which suggests that trace As atoms were indeed incorporated into the P sites.

The As K-EXAFS oscillations multiplied by k were Fourier transformed over the range $4 < k < 15$ Å^{-1}. Fig. 7 indicates the results for 0.1 ML As/InP and InAs powder. Prominent features observed at ~1.8–2.8 Å are due to the nearest-neighbor In atoms. Fig. 7 also shows the results of the Fourier transform for As impurities (7.3×10^{19} cm^{-3}) in InP and InAs powder (Oyanagi *et al.*, 1988). For 0.1 ML As/InP and As:InP, the positions of the nearest-neighbor peaks matched that of InAs. However, the magnitudes of the nearest-neighbor peaks for 0.1 ML As/InP and As:InP are greater than that of InAs by ~20%. In Fig. 8, the local structure of As atoms in a dilute limit is compared with that of a strained heterointerface.

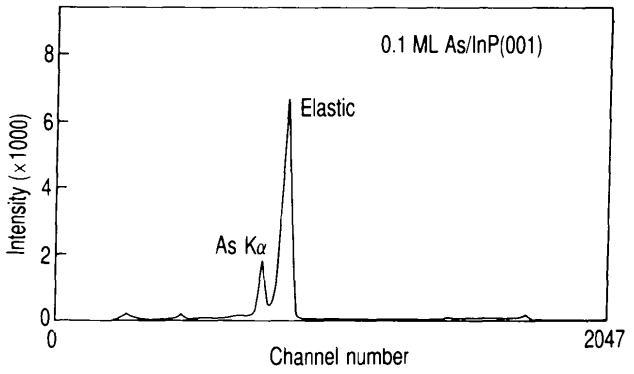

Figure 4
Fluorescence X-ray spectrum for 0.1 ML As on InP(001) capped by 20 Å InP. The elastically and inelastically scattered photons and characteristic X-rays from other elements which have lower absorption edges are the source of background.

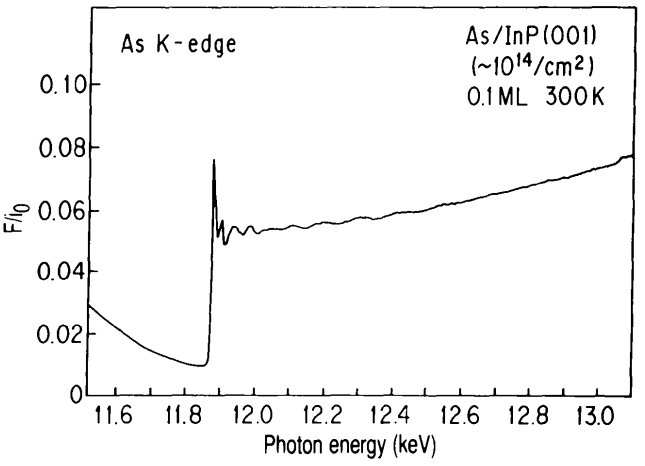

Figure 5
As K-edge fluorescence yield spectrum measured in surface-sensitive geometry using a 27-pole wiggler and a multi-element solid-state detector for 0.1 ML As/InP(001) capped by 20 Å InP.

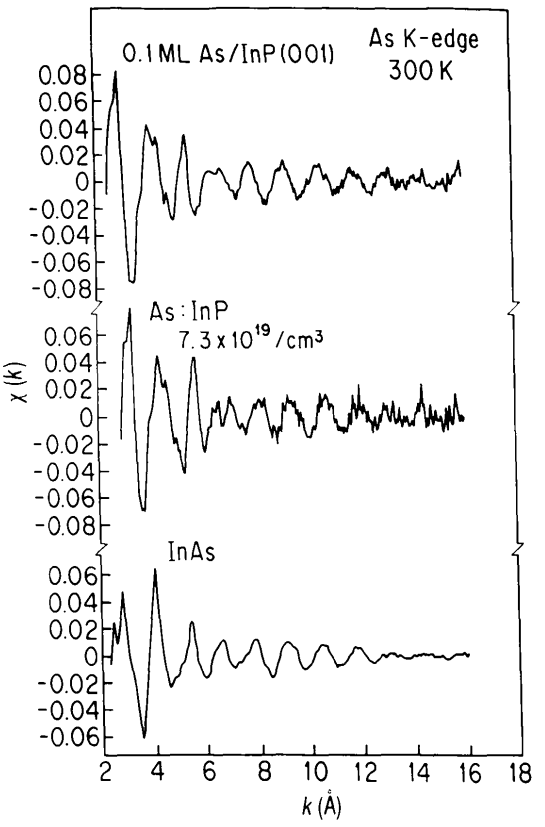

Figure 6
As K-EXAFS oscillations for 0.1 ML As/InP(001) (top), As:InP (middle) and crystalline powder InAs (bottom) plotted as a function of photoelectron wavenumber k.

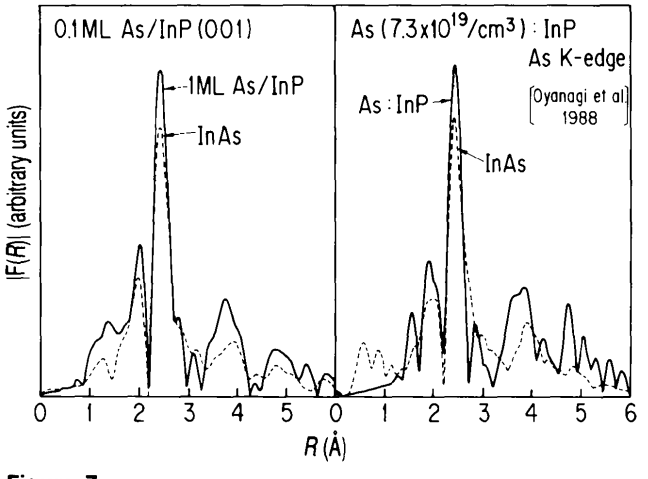

Figure 7
Magnitude of the Fourier transform of the As K-EXAFS oscillations multiplied by k for 0.1 ML As/InP(001) (left) and As:InP (right) (Oyanagi *et al.*, 1988). Dashed lines indicate the results for reference data for InAs powder.

4. Discussion

4.1. *Performance*

Although the potential of the multipole wiggler as a highly brilliant light source for rapid and sensitive XAFS has been recognized, until now the heat load problem has prevented its use in XAFS experiments since an energy resolution of 1–2 eV is essential for X-ray absorption near-edge structure (XANES) experiments. For a multipole wiggler beamline, the high heat load gives rise to various distortions of the crystal such as bend, local bump and graded lattice spacing (Oversluizen *et al.*, 1989). All these distortions broaden the width of the rocking curve and degrade the energy resolution. The first crystal used in the present study can handle the multipole wiggler radiation for $B_0 < 1.25$ T, corresponding to 70% of full power. The flux of a monochromated X-ray beam (9 keV) was compared with that of a bending magnet at BL4C at the Photon Factory. For a fair comparison, unfocused beam intensities with the same resolution ($\Delta E/E \simeq 2 \times 10^{-4}$) were compared. The results indicated that the photon flux at BL13 was 15 times greater than that of BL4C.

Various types of multi-element solid-state detectors have been reported based on a pure Ge element because of their superiority in energy resolution, packing fraction and convenience in packaging and maintenance (Cramer, 1991). We have developed the 7-element Si(Li) detector for fluorescence XAFS research, which is advantageous in that it is free from an 'escape peak' problem and a high count rate is easily obtained by choosing a proper feedback resistor. The detector output was found to be linear with respect to the intensity of the detected beam for up to 2.5×10^4 counts s^{-1} after dead-time correction according to a simple exponential expression. A similar value has been reported for the 13-element pure Ge detector (Murphy *et al.*, 1995). No degradation of energy resolution and energy shift was observed at the highest count rate. The total count rate to be handled by the present detector system is 1.8×10^5 counts s^{-1}. This indicates that the total fluorescence detection efficiency increased by more than two orders of magnitude compared with a bending magnet and a single-element solid-state detector.

Table 1
Structural parameters for the In—As bond in 0.1 ML As/InP.

Specimen	R_{In-As} (Å)	ΔR_{In-As} (Å)	σ (Å)
InAs powder	2.623*		0.053
As:InP	2.60† ± 0.01	0.023 ± 0.01	
0.1 ML As/InP	2.60 (5) ± 0.01	0.018 ± 0.01	0.049

* Determined by X-ray diffraction. † Taken from Oyanagi *et al.* (1988).

4.2. *Incorporation of As on InP(001)*

The In—As bond length R_{In-As} and the mean-square relative displacement σ_i were determined by a curve fit to the experimental data using the empirical total phase shift and the theoretical backscattering amplitude $|f_i(\pi, k)|$ for In (Teo & Lee, 1979). InAs powder was used as a reference material for extracting the phase-shift function for the In–As pair. The EXAFS oscillation for the As–In pair was filtered into a space by a back-Fourier transform and curve-fitted by a single-scattering formula. The results are summarized in Table 1 together with those for InP(20 Å)/1 ML InAs/InP(001), referred to 1 ML InAs/InP (Kuwahara, Oyanagi *et al.*, 1994).

The In—As bond length in 0.1 ML As/InP [2.61 (1) Å] coincides with that of As:InP [2.60 (1) Å] (Oyanagi *et al.*, 1988) and 1 ML InAs/InP [2.60 (1) Å] (Kuwahara, Oyanagi *et al.*, 1994) within experimental error. The In—As bond length in pure InAs (2.623 Å) is longer than the In—P bond length in InP (2.541 Å) by 3%. This bond-length mismatch causes various types of lattice distortion in pseudobinary alloys or strained superlattices. The In—As bond length shortened by ~0.88% in As:InP (Oyanagi *et al.*, 1988). A similar bond-length contraction has been observed recently for 1 ML InAs/InP (Kuwahara, Oyanagi *et al.*, 1994) and AsH_3-exposed InP(001) without PH_3 flow (Shioda *et al.*,

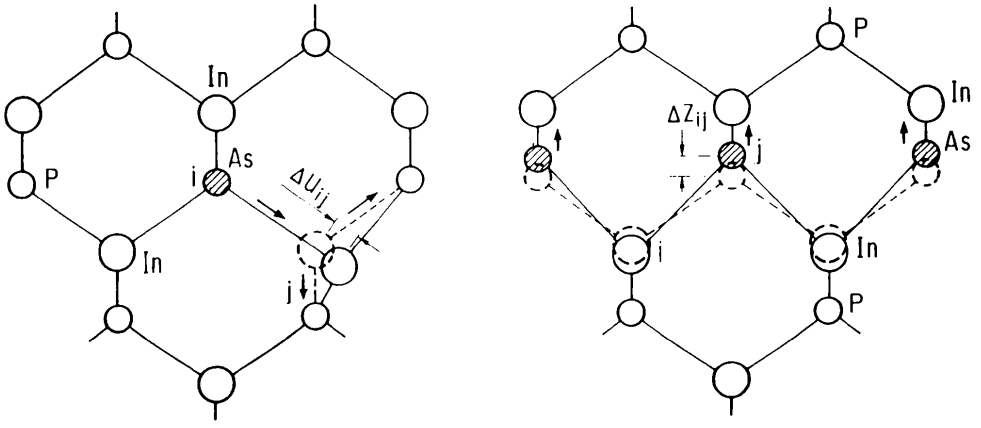

Figure 8
Schematic representations of the local distortions around an impurity (left) and a strained heterostructure (right). In a dilute limit, the mismatch in atomic size results in the isotropic displacement of nearest neighbors or bond-length shortening. For a strained heterostructure, the deformation is a two-dimensional displacement of interface atoms.

1994). It is reasonable that the local structure of trace As atoms incorporated into InP is essentially the same as that of As:InP. In a dilute limit, the doped isoelectric impurity atoms are dispersed in the host lattice and the probability of finding impurity atoms as the second-nearest neighbor is negligible. Interestingly, the magnitude of the nearest-neighbor displacement for 1 ML InAs/InP is the same as those for 0.1 ML As/InP and As:InP, although the nature of the local lattice distortion is quite different for the two cases, *i.e.* a dilute limit and a strained heterointerface.

Fig. 8 schematically illustrates the displacement of atoms around an As impurity in InP for a dilute limit and a strained heterointerface. In a dilute limit, the displacement of In atoms along the [111] direction, Δu_{ij} dominates the local distortion around As atoms and the variation of the second-nearest As—P distance is small (Oyanagi *et al.*, 1988). This also results in a simultaneous compression of the In—As bond length. In a dilute limit case, the mismatch is compensated by the isotropic displacement of the nearest-neighbor counter ions. However, in the case of a strained heterostructure such as 1 ML InAs/InP, the uniaxial compressive strain would cause the anisotropic displacement of atoms along the [001] direction since the in-plane lattice spacing is conserved. It is quite interesting that these two extreme cases of bond-length relaxation result in the same magnitude of bond-length shortening. This indicates that the magnitude of bond-length relaxation is not dependent on the dimensionality of the strain in extreme cases. This further suggests that the bond-bending relaxation dominates the lattice relaxation caused by the bond alternation. On increasing the number of As atoms occupying the adjacent second-neighbor sites on the same plane, however, the two types of displacements, *i.e.* those along the [111] and [001] directions, coexist in the same plane. This would increase the elastic energy of a strained layer which causes an anomalous bond contraction for 1 ML $InAs_{0.5}P_{0.5}$ (Kuwahara, Aono *et al.*, 1994)

It should be noted that the mean-square relative displacement observed for the trace As atoms in InP was always smaller than that of InAs. This is clearly seen in the Fourier transform results shown in Fig. 7: the magnitude of the first peak at ~2.2 Å for 0.1 ML As/InP and As:InP is greater than that of InAs powder by about 20%. Clearly, this is not caused by self-absorption correction effects which would apparently decrease the magnitude of EXAFS oscillations measured by a fluorescence mode. Instead, this indicates that the compressed In—As bonds become tight and the magnitude of thermal vibrations along the [111] direction decreases. The difference in the phonon density of states between InP and InAs may also cause such a difference. This will be clarified by analyzing the temperature dependence of a mean-square relative displacement.

4.3. *Capability as a surface structural tool*

Various surface-sensitive measurements of XAFS have been proposed. The reflectivity near the critical angle has been used to obtain the information for the sample surface within several hundred ångströms (Martens & Rabe, 1981). It was shown that normal incidence and grazing-exit geometry is an alternative means for surface-selective monitoring of fluorescence (Suzuki, 1989). Monolayer surface sensitivity was reported at atmospheric pressure using a photocathode detector (Long *et al.*, 1989). Recently, photocurrent measurement under a total reflection regime showed high surface sensitivity comparable with an Auger electron yield (Kawai *et al.*, 1993). The advantage of grazing-incidence fluorescence detection over these techniques is its versatility and sensitivity: it is a general means of monitoring surface-sensitive XAFS in a hard X-ray region, covering most elements heavier than Ca ($Z > 20$). Presently, the lower limit in energy (4 keV) is determined by the absorption due to the Be windows which seal the upstream ultra-high vacuum section and downstream section. This technique can be applied to surfaces consisting of light elements (Fischer *et al.*, 1986) if the absorption due to the Be windows is reduced. The same experimental set-up is used with other techniques such as surface X-ray diffraction (Marra, Eisenberger & Cho, 1979) or X-ray standing waves (Cowan, Golovchenko & Robbins, 1980). Lastly, we note that a high-brilliance beam from an X-ray tunable undulator at a third-generation synchrotron facility and a high-density multi-element solid-state detector would achieve rapid and sensitive XAFS measurements (Oyanagi, 1993) that would allow us to investigate the microscopic mechanism of growth and reaction kinetics.

5. Conclusions

In surface-sensitive geometry, the incident beam flux and detector efficiency are directly related to the sensitivity. The improved cooling efficiency of the directly cooled first crystal used in a 27-pole wiggler beamline achieved a tolerable energy resolution ($\Delta E/E \simeq 2 \times 10^{-4}$) for a maximum 70% of full power. The use of a multipole wiggler resulted in a 15-fold increase of incident beam flux over a wide energy range (4–30 keV). Combining a 27-pole wiggler and a 7-element Si(Li) detector, the efficiency of fluorescence detection increased by more than two orders of magnitude. Application to an InP(001) surface exposed to AsH_3 flow demonstrated that fluorescence detection in grazing-incidence geometry indeed has sub-monolayer sensitivity. It was found that ~0.1 ML As atoms are incorporated into the substrate within 0.5 s when PH_3 was kept flowing. This provides direct evidence for surface site exchange between the source gas materials and adatoms.

The authors express their thanks to H. Kitamura, M. Yamamoto, M. Hara, S. Sasaki, Be S. Hee and H. Kamitsubo for the design and construction of a 27-pole wiggler and a beamline front-end. The authors wish to express their thanks to H. Kamei for providing the AsH_3-exposed InP samples. They also thank the Toray Research Center for ICPMS analysis of the As coverage.

References

Becker, R. S., Golovchenko, J. A. & Patel, J. R. (1983). *Phys. Rev. Lett.* **50**, 153–156.

Cowan, P. L., Golovchenko, J. A. & Robbins, M. F. (1980). *Phys. Rev. Lett.* **44**, 1680–1683.

Cramer, S. (1991). *X-ray Absorption Fine Structure*, edited by S. S. Hasnain, pp. 640–645. Chichester: Ellis Horwood.

Fischer, D. A., Dobler, U., Arvanitis, D., Wenzel, L., Baberschke, K. & Stohr, J. (1986). *Surf. Sci.* **177**, 114–120.

Heald, S. M., Keller, E. & Stern, E. A. (1984). *Phys. Lett. A*, **103**, 155–158.

Jaklevic, J., Kirby, J. A., Klein, M. P., Robertson, A. S., Brown, G. S. & Eisenberger, P. (1977). *Solid State Commun.* **23**, 679–683.

Kamei, H. & Hayashi, H. (1991). *J. Cryst. Growth*, **107**, 567–572.

Kawai, J., Hayakawa, S., Kitajima, Y., Suzuki, S., Maeda, K., Urai, T., Adachi, H., Takami, M. & Gohshi, Y. (1993). *Proc. Jpn. Acad. Ser. B*, pp. 179–184.

Kuwahara, Y., Aono, M., Shioda, R., Oyanagi, H., Takeda, Y., Haga, K. & Kamei, H. (1994). In preparation.

Kuwahara, Y., Oyanagi, H., Shioda, R., Takeda, Y., Yamaguchi, H. & Aono, M. (1994). *Jpn. J. Appl. Phys.* **33**, 5631–5635.

Long, G. G., Fischer, D. A., Kruger, J., Black, D. R., Tanaka, D. K. & Danko, G. A. (1989). *Phys. Rev. B*, **39**, 10651–10657.

Marra, W. C., Eisenberger, P. & Cho, A. Y. (1979). *J. Appl. Phys.* **30**, 6927–6933.

Martens, G. & Rabe, P. (1981). *J. Phys. C*, **14**, 1523–1534.

Murphy, L. M., Dobson, B. R., Neu, M., Ramsdale, C. A., Strange, R. W. & Hasnain, S. S. (1995). *J. Synchrotron Rad.* **2**, 64–69.

Oversluizen, T., Matsushita, T., Ishikawa, T., Stefan, P. M., Sharma, S. & Mikuni, A. (1989). *Rev. Sci. Instrum.* **60**, 1493–1500.

Oyanagi, H. (1992). *Proceedings of an International Symposium on Optical Applied Science and Engineering*. Washington, DC: SPIE.

Oyanagi, H. (1993). *Jpn. J. Appl. Phys.* **32**(Suppl. 2), 861–865.

Oyanagi, H., Kuwahara, Y., Yamaguchi, H. & Shioda, R. (1995). In preparation.

Oyanagi, H., Sakamoto, T., Sakamoto, K., Matsushita, T., Yao, T. & Ishiguro, T. (1988). *J. Phys. Soc. Jpn*, **57**, 2086–2092.

Oyanagi, H., Takeda, Y., Matsushita, T., Ishiguro, T., Yao, T. & Sasaki, A. (1988). *Solid State Commun.* **67**, 453–458.

Sasaki, S., Yamamoto, S., Shioya, T. & Kitamura, H. (1989). *Rev. Sci. Instrum.* **60**, 1859–1862.

Shioda, R., Oyanagi, H., Kuwahara, Y., Takeda, Y., Haga, K. & Kamei, H. (1994). *Jpn. J. Appl. Phys.* **33**, 5623–5629.

Suzuki, Y. (1989). *Phys. Rev. B*, **39**, 3393–3395.

Teo, B. K. & Lee, P. A. (1979). *J. Am. Chem. Soc.* **101**, 2815–2832.